SEPARATION POSTPONEMENT BY MEANS OF PERIODIC SURFACE EXCITATION

L.L.M. Veldhuis , M. van der Jagt
Delft University of Technology

Keywords: *separation control, vortex generators, surface excitation*

Abstract

In this paper we discuss the separation control capabilities of surface excitation actuators. Their effect is compared to the effects of standard vortex generators (VG) as well as Micro-Vortex generators by performing pressure and PIV measurements on the flow over a ramp. In the experiments the actuators proof to have the same separation control capability as standard VGs while Micro-VGs perform a little bit better. Furthermore CFD calculations were performed on a wing-flap model in which the separation over the flap was controlled. The results show that a lift increase of around 18% can be obtained compared to the model without actuator.

1 Introduction

Flow separation on an airfoil has serious consequences in the form of significant loss of lift combined with an increase in drag. To counteract flow separation, many passive and active separation control devices have been investigated in the past. The passive device mostly investigated and applied in aerospace applications is the the vane type vortex generator (VG). This passive device has shown to be quite effective but its fixed presence in the flow leads to unwanted drag increase for low angles of attack where flow separation is absent. It is this disadvantge of VG's that has led to increased interest in active control techniques where the actuator can be switches on only when it is needed.

Amongst the active flow control techniques that have been studied during the last decades some attention was paid to periodic surface excitation [1, 2, 3, 4, 5, 6]. The system is based on a periodically moving surface that leads to vortex shedding such that separation is postponed. However, the question remain as to how effective periodic surface excitation is with respect to other methods like VG's. Although additional research has become available [5] which shows that periodic excitation works over the entire Reynolds range that is covered by aircraft, it is still unclear how the postponement of separation is established.

The aim of this research is to compare the effectiveness of periodic surface excitation with the effectiveness of vortex generators. Furthermore in this research a further insight is obtained on the phenomena that lead to postponement of separation. The comparison is based on experimental research on a two-dimensional test setup using various techniques like surface pressure measurements and Particle Image Velocimetry (PIV). Additionally , some preliminary CFD calculations are presented which show that flap-type surface actuators (denoted *fliperons*) are capable of performance improvement of wing flap systems where large flap angles are employed.

2 Experimental setup and test approach

2.1 Windtunnel and model

Separation was provoked on the top of a ramp that was placed inside the Boundary Layer Windtunnel (BLT) of the Faculty of Aerospace Engi-

neering of Delft Universty of Technlogy. This windtunnel was specifically designed for research on laminar boundary layers and transition. The windtunnel consists of a closed circuit that has been equiped with silencers to remove noise that may detrimentally influence boundary layer transition. The lower wall (which is used for measurements in the boundary layer) is basically a flat plate with a length of $L_p = 5.6\,m$ and a width of $W_p = 1.5\,m$. At its leading edge the incoming wall boundary layer is removed through a sharp edged slot.

To generate a specified pressure distribution the upper wall (which is separated from the lower wall approximately $0.25\,m$) can be curved over its complete length. Flow separation as well as variation in the effective cross sectional area due to boundary layer development on the curved wall is prevented by removal of the boundary layer through a system of slits and suction chambers behind the wall. The main reason for selecting this windtunnel is the fact that it guarantees a high quality two-dimensional flow. In earlier investigations flow separation over flaps has proven to be very unstable (generating 3D vortices) in case the flap chord to tunnel width ratio becomes to small [1].

The maximum windspeed in this facility is $V_{max} = 45\,m/s$ with a flow turbulence level of about 0.09% , when measured at a distance of 1 meter from the leading edge of the lower wall [7]. For additional information on the BLT the reader is referred to van Hest, [8].

The ramp model that was used during this research is based on a simplification of a wing with trailing edge flap as sketched in fig. 1. Although this approach may have some restrictions, the given setup allows easy manufacturing and adaptation as well as low CFD modeling effort as compared to a real wing flap system. An overview of the test setup and the ramp design is shown in figure 2.

The boundary layer was made turbulent by means of a zigzagged transition strip attached close the leading edge of the (lower) test wall. Due to its layout the separation point was fixed at

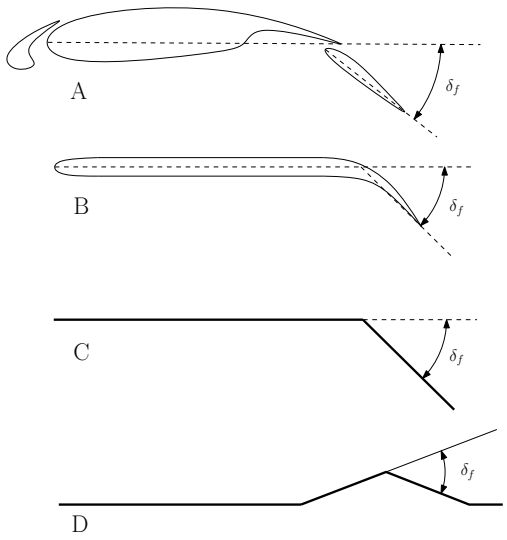

Fig. 1 Model simplications; (a) Typical high lift airfoil model, (b) Simplicated model with curvature, (c) Corner flow, (d) Ramp flow

the top of the ramp, as shown in fig. 2b.

2.2 Flow control devices

Two types of flow control methods were tested: vortex generators and periodic surface excitation. Their effect on separation postponement was determined using: pressure measurements, tuft visualization and 2D PIV measurements.

2.2.1 Vortex generators

The most important VG design parameters are: the height (h), the vane spacing (s), the VG spacing (λ) and the angle of incidence (β). These parameters are shown in fig. 3. Finally the distance between the VG's and the separation point (x_s) is of major importance. Based on the successful results found in earlier investigations [1, 9, 10, 11] , two heights of the VG were chosen. For the *standard VG* the height is equal to the local boundary layer thickness, $h = \delta$. The smaller version, denoted Micro-VG, has a height of $h = \delta/2$. This Micro-VG has shown a large potential in the control of separation. The main reason to decrease the height of the vortex generator is that they produce less drag than the standard VGs.

To reduce the number of variables to be investigated, the VG angle of incidence was fixed

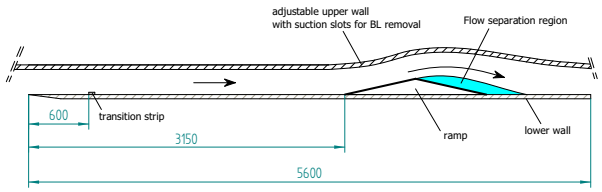

(a) General overview of the ramp inside the Boundary Layer windtunnel (dimensions in mm)

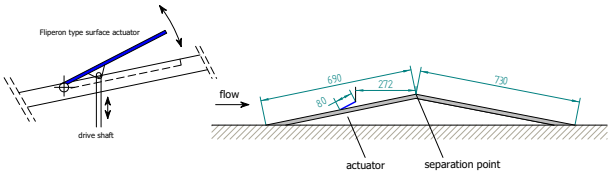

(b) Location of the actuator on the ramp (dimensions in mm)

Fig. 2 Experimental setup.

at 17 deg. This angle is in accordance with the optimum value found by others [9].

2.2.2 *Surface excitation device*

The actuator that was used consists of a small plate that is hinged at its leading edge denoted as a 'fliperon' (fig. 4). An attractive way of driving the actuator is by using Piezoelectric elements [4, 12]. One disadvantages of Piezoelectric actuators is the limited deflection (A) that can be attained in case they are applied as a flat element lying on the surface.

In the current investigations a rather thick boundary layer ($\delta = O(40mm)$) was produced to be able to perform detailed flow measurements in the viscinity of the actuator. After a feasability analysis it appeared that the combination of deflection and frequency necessary for the experiment could not be reached with available piezoelectric materials. Even if the piezo-electric actuator resonated at its eigenfrequency the required deflection was not reached. Therefore a mechanically driven actuator was applied that consists of an electrical motor that drives a small shaft in a direction perpendicular to the surface.

For the actuator the location was fixed upstream of the separation point. The parameters varied were the frequency, f, and the amplitude, A. Besides this several surface shapes (like

Conventional VG (left) and Micro-VG (right).

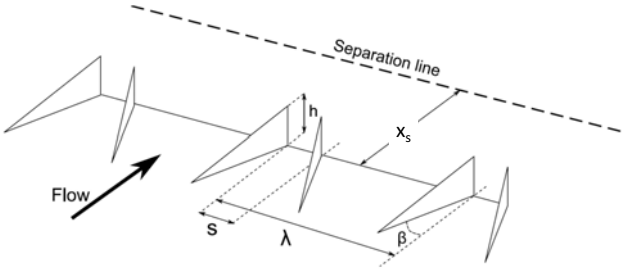

VG design parameters.

Fig. 3 Vortex generator layout and parameters.

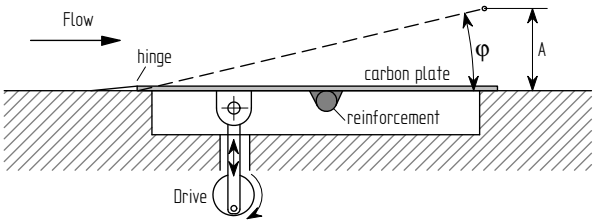

Fig. 4 Surface excitation actuator layout ('fliperon').

straight and serrated trailing edge flaps) were tested.

2.3 Measurements

Pressure measurements Pressure measurements were performed along the complete wall. In total 48 static pressures were measured; 36 on the windtunnel wall and 12 on the ramp. The spacing between the pressure orifices is 10*cm* for the orices on the wall and approximately 8 to 9*cm* for the orifices at the ramp. Pressure measurements in the boundary layer were performed in two different ways: by means of a boundary layer rake and by traversing a boundary layer probe.

Tufts visualization In addition to pressure measurements, tuft measurements were carried out. These data were used to check the intrepretation of the measured pressure data that were sometimes inconclusive. Because the tuft is extremely exible, it will point in the direction of the flow. Since the view to the inside of the tunnel was limited, the images that where taken from the side were dewarped manually. Fig. 5 shows a typical tufts pattern at the backside of the ramp clearly indicating a recirculation area.

PIV measurements The flow phenomena that occurred in all test cases as well as separation postponement capabilities of the actuators were investigated by PIV measurements in the vicinity of the actuator. The system consisted of a 200 mJ Quantel Twins CFR-200 double pulse ND:Yag laser combined with 2 CCD cameras with 1280x1024 pixels resolution. The maximum sampling rate that was attainable with this

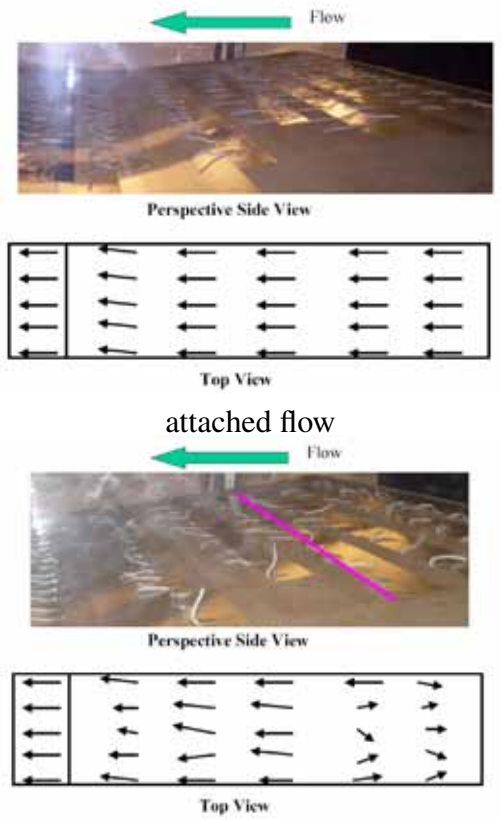

Flow reattachment on back of the ramp

Fig. 5 Example of tuft images taken at the back of the ramp. In (b) the reattachment point is found close to the cyan colored line.

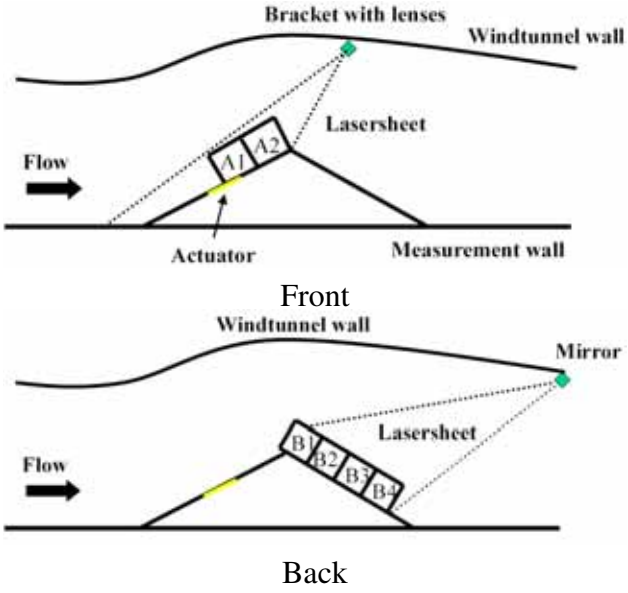

Fig. 6 Overview of PIV field that were taken over the ramp.

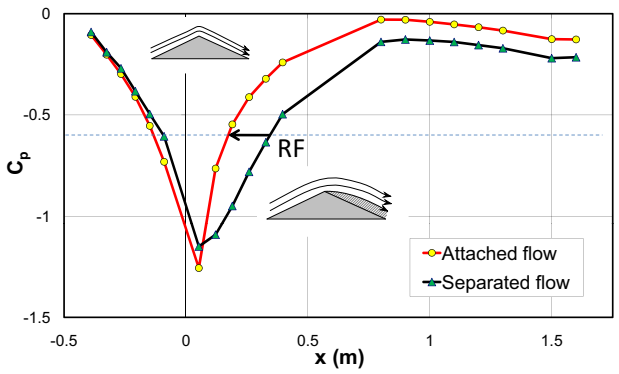

Fig. 7 Definition of the recovery factor: the distance between the pressure distribution for the control device and the distribution for the separated flow at $c_p = -0.6$.

system was 3.3 Hz. Seeding of the flow was done using a Safex Twin Fog Generator which produced particles of approximately 1 μm diameter.

3 Experimental results

3.1 Pressure data

3.1.1 Vortex Generators

The performance of the surface actuator and the vortex generators was quantified by a recovery factor that is based on a shift of the pressure distribution associated with the separation profile [1]. This recovery factor, RF, was taken at a *fixed* value of the pressure coefficient $c_p = (p - p_0)/q_0$. Here p_0 and q_0 are respectively the static pressure and the dynamic pressure taken at the beginning of the test section (at the location of the lower wall leading edge). The interpretation of the pressure plot using RF illustrated in fig. 7. The recovery factor is made non-dimensional by dividing it by the length of the ramp.

From the experiments the following recovery factors were found:

1. $RF = 0$ for completely separated flow
2. $RF = 0.52$ for fully attached flow
3. $0 < RF < 0.52$ for a reattachment line that is located on the ramp

Comparison with the tuft patterns that were recorded for all configurations showed that RF is indeed an accurate indicator of the status of the ramp boundary layer.

Prior to the comparison between VGs and surface actuator the position and layout of the VGs was optimized. For test with variable distance, x_s, from the separation point (fig. 8a) the standard VGs show an optimum $x_s \approx 20\delta$. The Micro-VGs perform best when they are placed at 2.5δ in front of the separation point. Both curves show the same behavior, but the Micro-VG curve slope is larger. This directly shows an important aspect of Micro-VGs; although they perform better than the conventional VGs, they are more sensitive to the location on which they are placed. An optimal distance is found because when the distance to the separation point becomes too large, the vortices dissipate too fast to be effective. When the distance becomes too short, the vortices are not well developed yet.

After the optimal distance was determined, the vane spacing was varied. The recovery factors can be found in fig. 8b. For both cases an optimum was found. For the conventional VGs an optimum value of $s = 3\delta$ was found whereas for the sub-VG's a value of $s = 1.5\delta$ was found.

Table 1 Comparion of optimum VG parameters.

Standard VG's

Source	D	x_s	β
Taylor [10]	$4.8-12\delta$	$10-30\delta$	16^o
Artois[1]	6.7δ	$20-30\delta$	16.7^o
Current research	7δ	20δ	17^o

Micro-VGs

Source	h	D	x_s	β
Lin [11]	$0.2-1.0\delta$	$5h$	$5-10h$	23^o
Current research	0.5δ	$6.5h$	$6h$	17^o

The reason for the existance of an optimum value is as follows. When the distance between the VGs becomes too small, the counterrotating vortices are going to merge, reducing each other's strength. However, for too large a distance, a region between the vortices exists which is not reenergized.

Finally the VG spacing is varied. The graphs for the recovery factors are shown in fig. 8c. For the conventional VG's an optimal value of $\lambda = 2.5$ was found whereas for the Micro-VGs $\lambda = \delta$ is optimum.

The optimum values found in this research are compared to values found by other researchers. Instead of working with λ and s, it is common to work with a parameter D, which is the 'effective distance' between to VG pairs, defined as

$$D = \lambda + s + 2l\sin\beta$$

Table 1 gives a comparison of the optimum values found for both the standard VGs and the Micro-VGs.

As can be seen from the table, the values are in the same range. The fair agreement between the data also indicates that the somewhat arbitrary defined recovery factor is indeed a good measure for finding the optimal configuration.

3.1.2 Surface actuator

In total four different actuator shapes were evaluated (fig. 9). Type A is based on the piezoelectric actuators used by other researchers, [26]. Here no

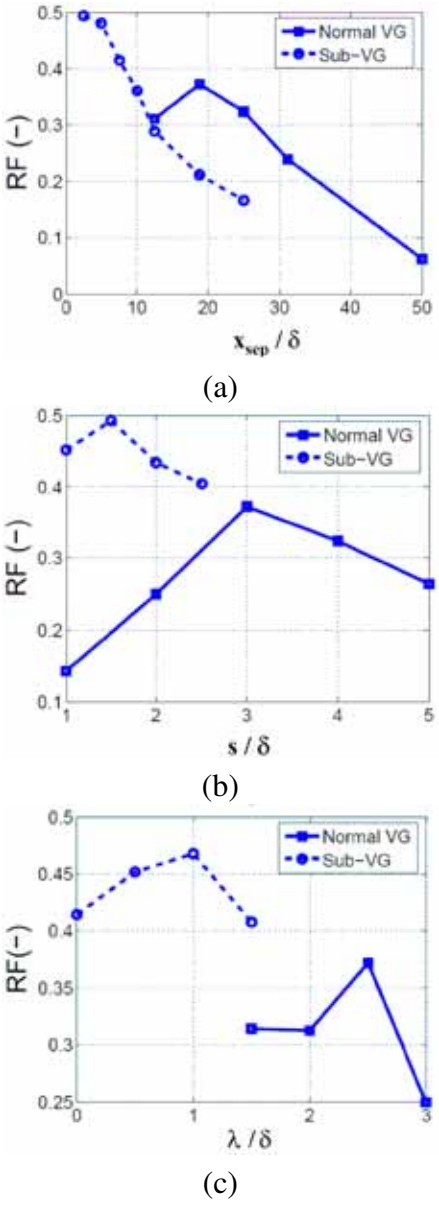

Fig. 8 RF as a function of the distance to the separation point (a), the vane spacing (b) and the VG spacing (c).

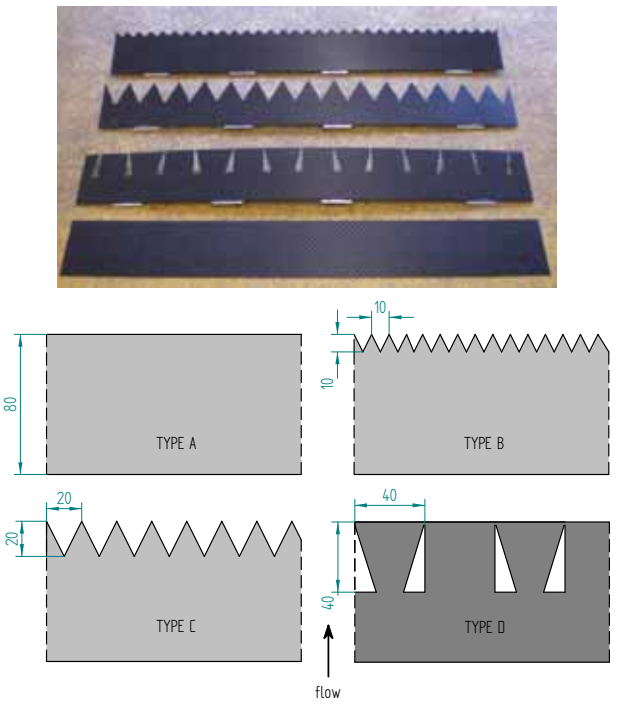

Fig. 9 Different shapes of the actuator tested.

cut out was made and when viewed form above, the shape is rectangular. Type B and C are actuator surfaces with a cut out of a triangular shape. As shown in fig. 9b, the cut out of type B consists of small triangles, whereas the cut out of type C consists of large triangles. As a fourth type, an actuator surface with a cut out based on the vortex generator shape was used. This is indicated by type D. These designs were based on a survey conducted by Osborn [13].

During the measurements the actuator shape, the reduced frequency, F^+, and the deflection, A were varied. The reduced frequency that is used herein is defined as:

$$F^+ = \frac{fX_{te}}{U_\infty}$$

Here X_{te} is the distance between the actuator and the location over which the periodic disturbances should remain effective. In this set-up this distance was determined as being $0.9m$. The value of $F^+ = 0$ corresponds to a fixed static deflection.

In fig. 10 the effect of F^+ on the recovery factorare are shown for different amplitudes. The maximum RF that was attained with the VGs is plotted as horizontal lines ($RF = 0.37$ for standard VGs, $RF = 0.49$ for Micro-VGs). From the graphs several conclusions can be drawn:

- Type A and type D perform better than types B and C
- Except for the smallest amplitude, ($A = \frac{2}{5}\delta$), the performance of the actuator can match the performance of the VGs
- The best results are found around $F^+ = 1.4$
- The curves have not yet reached their optimum. This is due to structural limitations which prevented the use of larger excitation frequencies.
- The limit value of RF is smaller than the maximum value found for the Micro-VGs
- The largest RF is found at $A = \frac{5}{4}\delta$, although the difference with $A = \delta$ is only marginal

As can be seen from the graphs a cut out in the surface causes a decrease in performance. This is very likely the result of a weaker lateral vortex that is produced due to a smaller effective area. As shown in the graphs, the RF values of type D are almost the same as the values for type A. The reason for this is that there is still a relatively large area which is not affected by the cut outs. Here a vortex similar to the vortex formed by the plane shape is created. The process of the vortex formation will be discussed in more detail in the next section, where the PIV results are described. The largest value of RF is found at F^+ of 1.4. However the graphs approach a limit value. This is in agreement with the findings of Nishri and Wygnanski [4], who found an optimum $F^+$of 1.5 on a wing flap combination with a actuator ('fliperon') positioned on the shoulder.

The variation of the maximum value of RF (at $F^+ = 1.45$), with the amplitude is shown in fig. 10e. There is a linear part up to $\frac{A}{\delta} = 1$. Above this value still an increase in performance can be

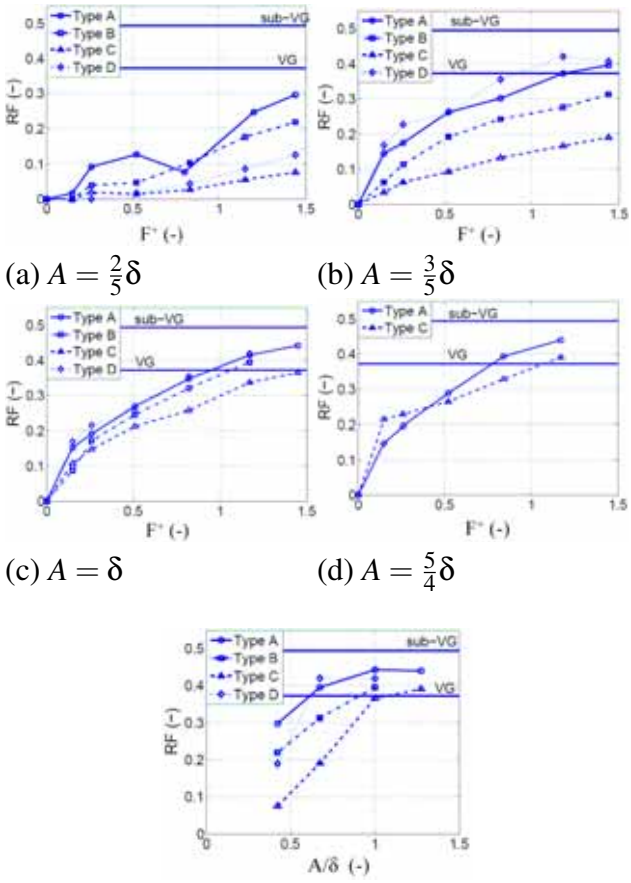

(a) $A = \frac{2}{5}\delta$ (b) $A = \frac{3}{5}\delta$

(c) $A = \delta$ (d) $A = \frac{5}{4}\delta$

(d) $F^+ = 1.45$

Fig. 10 Comparison of the recovery factor, RF , for different values of the actuator deflection (a) to (d) and different deflections of the actuator for a fixed F^+, (e).

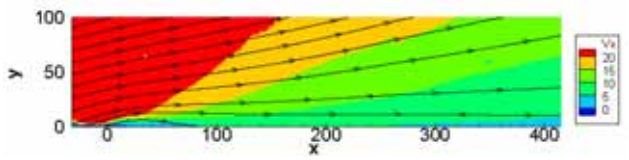

(a) Contourplot of V_x of the actuator. The actuator operated at $F^+ = 1.12$ and $A = \frac{5}{4}\delta$.

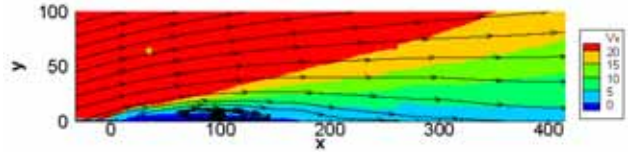

(b) Contourplot of V_x of the conventional VG at the optimal configuration.

Fig. 11 Comparison of the x-component of the velocity, V_x, between the flow at the back side of the ramp for the actuator (a) and the conventional VG (b).

seen but the gradient gets quite smaller. The large slope of the linear part shows a large sensitivity to the amplitude, especially when A is smaller than δ (it is therefore advised to ensure a minimal amplitude of $A = \delta$ in practical applications) . An important finding is that the performance of the given actuator can match the performance of the standard VGs. In fact in these experiments, where an almost perfect 2D flow was present, it was found that the performance of the actuator is even slightly better. However the performance of the Micro-VG's remain superior.

3.2 PIV data

The conclusion that the actuator is more effective than the standard VG is supported by PIV images at the back side of the ramp. Figure 11 shows the time averaged PIV images of the actuator (type A) and the VG. The PIV image of the VG (11b) shows that a separation bubble is still present on the back side of the ramp. On the other hand, the actuator eliminates flow separation completely (fig. 11a).

Averaged PIV images of the vorticity in the vicinity of the actuator are shown in figure 13. The process of obtaining the averaged value is sketched in fig. 12 . The PIV images were not

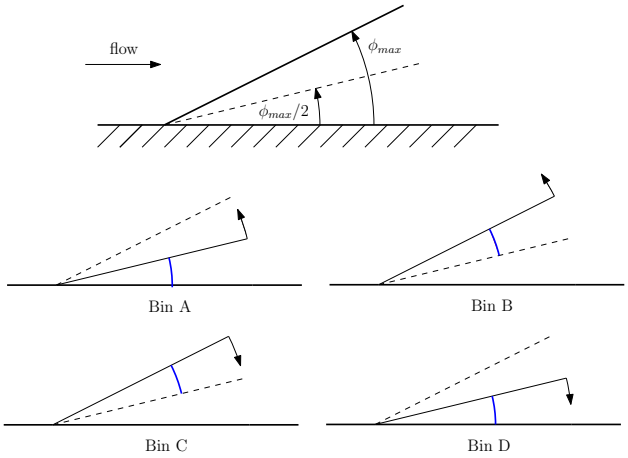

Fig. 12 Definition of the bins based on the actuator position, used to average the PIV images.

obtained with a triggered camera system (trigger system failed). Hence the images where 'binned' in 4 bins A to D.

Since the images are averaged, the actuator surface is marked with a black band. When the actuator moves up (images 13b and 13c) a discrete vortex is shed. When the actuator moves down, the vortex is stretched and convected with the flow. The images indicate that the vortex is composed of smaller scale structures. This was validated by instantaneous PIV images (fig. 14). A sketch of the typical vorticity patterns that is produced by the actuator is presented in fig. 15.

To enable a comparison with other investigations, the oscillatory momentum coefficients for our data were determined from the PIV data. The momentum coefficient is defined as:

$$c_\mu = \frac{1}{\frac{1}{2}U_\infty^2 L}\int \left(u'(y)\right)^2 dy$$

Here U_∞ is the freestream velocity, $u'(y)$ the fluctuating component of the horizontal velocity and L a reference length. In many investigations the chord of the airfoil is chosen for the reference length. This is generally based on a partly separated flow over the upper surface of the airfoil. Therefore in our case the ramp is considered as the part of the airfoil where separation takes place and length is take $L = 5m$. The result of the analysis of c_μ at various streamwise location is

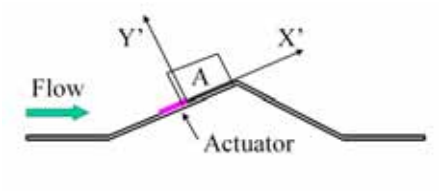

(a) Location of the measurement plane where the PIV images were taken.

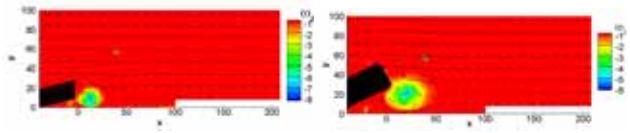

(b) Moving up, $t = t_1$.

(c) Moving up, $t = t_2$.

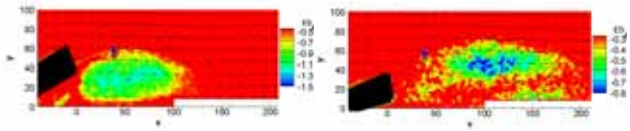

(d) Moving up, $t = t_3$.

(e) Moving up, $t = t_4$.

Fig. 13 Contourplots of $\omega_z \cdot 10^2$. In (b) and (c) the actuator moved up. In (d) and (e) the actuator moved down. All images are raw data. Due to averaging the view blocked by the actuator appears as a band, shown in black.

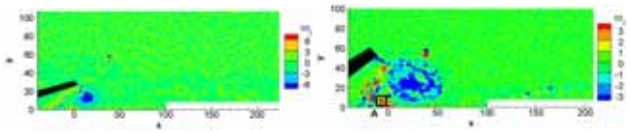

(a) Actuator at $\phi = \phi_{max}/2$, moving up

(b) Actuator at $\phi = \phi_{max}$, moving up

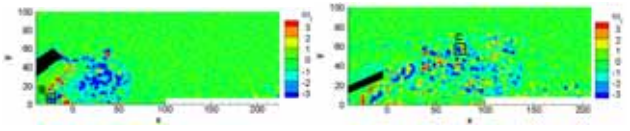

(c) Actuator at $\phi = \phi_{max}$, moving down

(d) Actuator at $\phi = \phi_{max}/2$, moving down

Fig. 14 Development of the coherent structures. Instanteneaous PIV data.

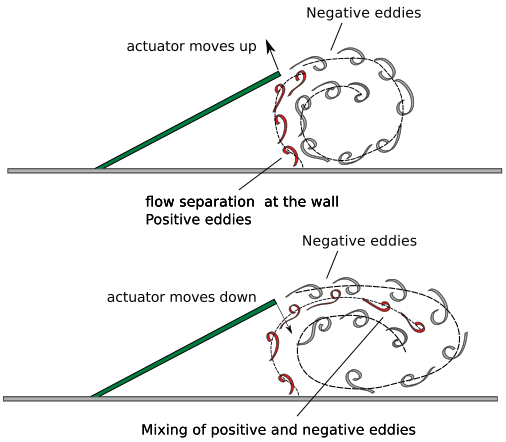

Fig. 15 Sketch of the formation of vorticity field behind the actuator where positive and negative values are found.

Table 2 Calculated values of c_μ at different streamwise positions.

Dist. from actuator (mm)	20	40	60	80	100
c_μ	296	275	156	110	65

presented in table 2. Here a freestream velocity of $18m/s$ was used. The same order of magnitude is found in other surface excitation methods. For example Nishri and Wygnanski [4], report a range of $60\times10^5-140\times10^5$ for the value of c_μ at the optimal reduced frequency. Furthermore in the research of Artois [1], a maximum value of 40×10^4 is reported behind the trailing edge of the actuator.

4 Numerical model

To check the effect of a possible surface actuator on the flow separation over a wing flap combination a CFD analysis was performed. Experimental research on such a model leads to serious actuator problems when high Reynolds numbers are to be simulated in a windtunnel. This can simply be seen from an example. Assume flow control in a windtunnel test over a flap of $0.15m$ chord in a wind speed of $V=80m/s$. Based on an optimum reduced frequency of $F^+=O(1.4)$ the required actuator frequency will be approximately $750Hz$. Using Piezo-lectric actuation (or

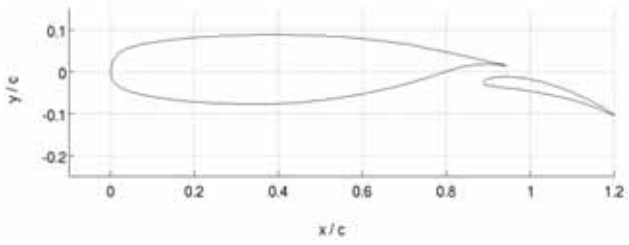

(a) Original NLR7301 airfoil.

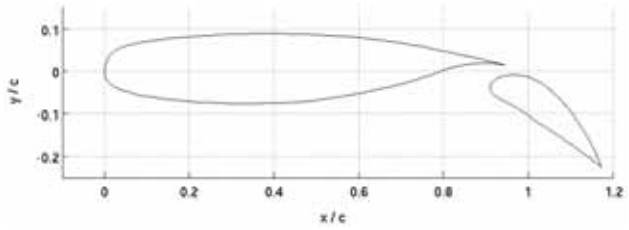

(b) NLR7301 with adapted flap.

Fig. 16 Original and adapted (flap) of the NLR7301 airfoil (different flap deflections in this figure).

any other means) it will be very difficult to reach this high frequency combined with a high enough actuator deflection. This is serious limitation (not to say show stopper) of the surface excitation actuator.

Nevertheless a simulation of the investigated actuator was performed so find out whether application on a wing flap would lead to performance improvement [15]. The goal in this case is to apply large flap deflections to enhance the lift coefficient of the model. The flow separation that occurs on the flap is then controlled by a surface actuator.

4.1 CFD Model

The model that was investigated is based on the NLR7301 airfoil with flap (fig. 16) that was tested in the Low Speed Windtunnel of the National Aerospace Laboratory (NLR) [1]. One of the goals of these tests was to provide sufficient data to allow validation of CFD codes. All calculations were performed with a commercial RANS solver (Fluent). Before the final calculation with the fliperon were performed the effect of the available turbulence models were investigated on the original baseline model (16a). A very good agreement between experimental

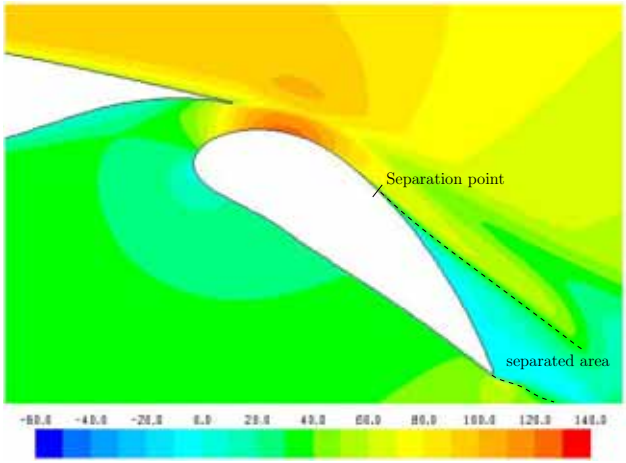

Fig. 17 Contour plot of the x-velocity. On the adapted congfiuration flow separation does not occur on the first half of the flap surface.

and numerical results was found for the baseline model. For details the reader is referred to Dolle [15].

It was found that for the the original flap the flow separates directly from the flap LE due to its very strong curvature. Since this leads to difficulties of implementing a surface actuator of finite chord, it was decided to redesign the flap (fig. 16b).

The actuator was simulated by applying a so-called *dynamic mesh* that adapts itself in time in accordance with the movement of the flap. All calculations were performed at a chord based Reynolds number of $Re = 4.0 \times 10^6$.

As is shown is fig. 17 the flap shows partly separated flow away from the leading edge allowing an actuator to be placed upstream.

The effects of three different actuators was investigated. Earlier investigations showed that the cavity underneath the gap plays a role in the effectiveness of the actuator [1]. The layout of the simulated actuators is sketched in fig. 18.

4.2 Results

An overview of all simulations that were performed is given in table 3.

From this table it follows that the dimensionless frequencies needed here are unexpectely much larger than the dimensionless frequencies

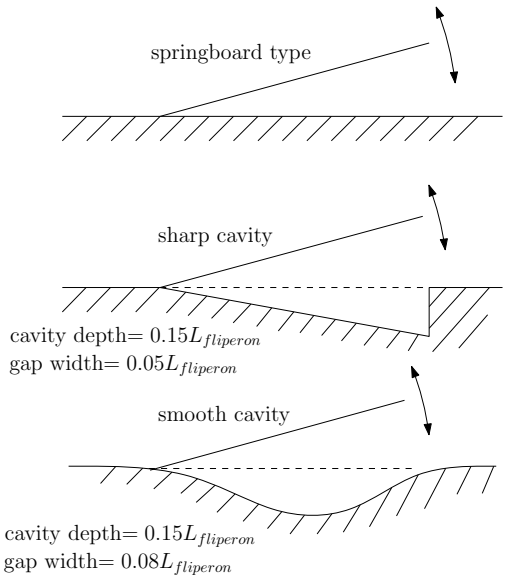

Fig. 18 Overview of the different fliperon-cavity geometries applied on the flap.

Table 3 Overview of performed simulations.

Type	Motion #	Oscillations	F^+	$\frac{A_{max}}{\delta}$
springboard	I	64	4.0	1.2
	II	143	6.0	1.2
sharp cavity	I	19	4.0	1.0
	II	86	6.0	1.0
	III	119	8.0	1.0
smooth cavity	I	104	4.0	1.0
	II	161	6.0	1.0
	III	127	8.0	1.0
	IV	98	10.0	1.0

applied on the experimental models. Apperently the high values of F^+were necessary because the pressure gradients on the flap are very high. This causes a stronger flow separation, which will require a larger momentum input and thus stronger vortices to reattach the flow to the flap surface.

In fig. 19 the calculation results of the springboard type actuator are presented for a flap deflection of $\delta_f = 60^0$.

At first instance, the lift coefficient decreases due to additional separation caused by the fliperon motion. When the first vortices arrive at the flap trailing edge, the lift starts increasing. It should be noted that the minimum allowable fliperon deflection for the springboard type was about 5^o due to the neccesity to have at least 2 layers of cells below the actuator. When enough vortices have passed the trailing edge, the system is fully developed and the lift coeffcients converges slowly. In case of motion I the lift coecient increases from 2.97 to 3.21, which is an increase of 8.0%. However, motion II turned out to result in a much better fliperon performance: the lift coecient increases to 3.50, which is an increase of 18%. For motion II the momentum coefficient was calculated to be much larger which support the findings in fig. 19.

In fig. 19b and c the vorticity field is shown for both motion I and motion II. These are instantaneous pictures of the vorticity, both taken at a moment the fliperon was at its lowest position. It can be seen that motion II, with the highest frequency, results in the production of smaller and stronger vortices. These vortices are able to reach the flap trailing edge, while the vortices produced by motion I separate from the flap surface more upstream. The main difference is found in the so-called secondary vortices. When the fliperon moves up, a large vortex is formed between the fliperon and the flap surface. At the beginning of the downward motion, this primary vortex leaves the fliperon and starts rolling over the flap surface. However, at the tip of the fliperon a second, smaller vortex is formed. In the case of motion I, this vortex is weak and lies more or less on top of the first vortex. These secondary vortices do not have a large in influence on the first vortices that

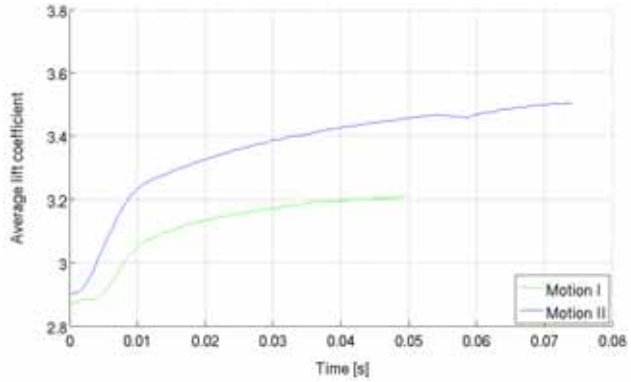

(a) Development of the lift coefficient in time.

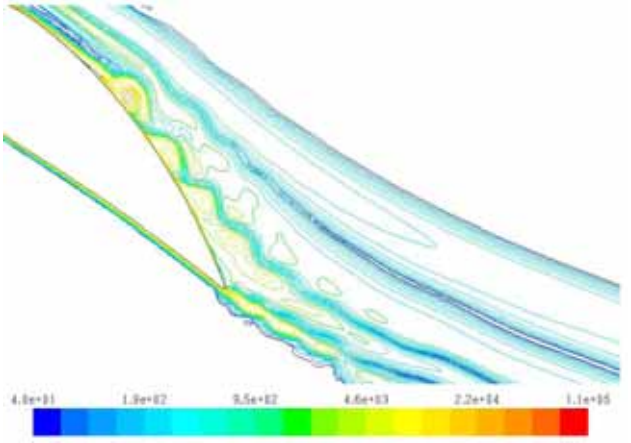

(b) Motion I

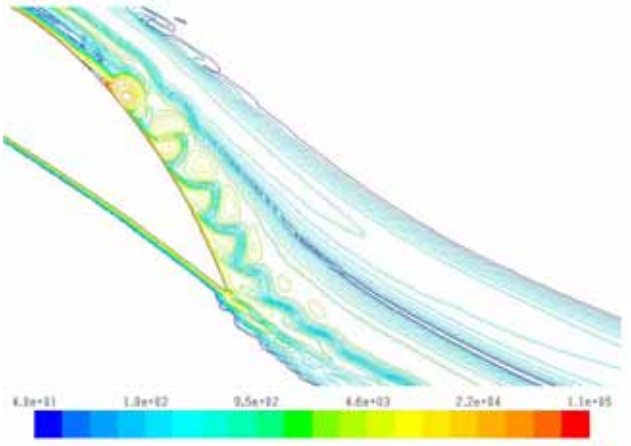

(c) Motion II

Fig. 19 Time history of the lift coefficient (a) and vorticity field over the flap (b,c) produced by the springboard type fliperon (b,c). The contours indicate the vorticity magnitude in s^{-1}.

roll over the surface. However, in case of motion II the secondary vortex is quite strong. Although these vortices do not roll over the surface, they fit exactly between the primary vortices. This might help to keep the primary vortices attached to the surface and let them reach the trailing edge. It can be seen that motion II is the most effective, since the resulting trailing edge vortices and the flap wake are much smaller.

In fig. 20 and 21 the development is presented for the sharp cavity and the smooth cavity respectively.

In the case of the sharp cavity the actuator produces a second vortex during the downgoing movement at the back side of the cavity. This vortex interacts with the primary vortex and prevents it from moving to far from the wall. The result is a larger gain in the lift coefficient for the optimum motion (III).

The design of the smooth cavity was based on the expectation that an increased push of the flow in streamwise direction would enhance the momentum transfer to the separated boundary layer. Therefore the sharp edge at the back of the cavity was smoothed to prevent the second vortex. As can be seen from the data in fig. 21 the expected performace increase is indeed found for motion II. The lower performace of motion IV is probable due to bursting of the wake of the main element as can be noticed at some distance away from the flap surface on the upper side.

The results of the CFD calculations are summarized in table 4. As expected both the reduced frequency as well as the presence of a cavity have a significant influence on the results. Especially the lift performance of the smooth cavity actuator is interesting.

Although the presented surface actuators have the advantage of not changing the structural integrity of the wing significantly it is unclear whether or not they can be applied in practice since:

- their reliability and maintainability may cause problems
- the need for high frequency (piezo-

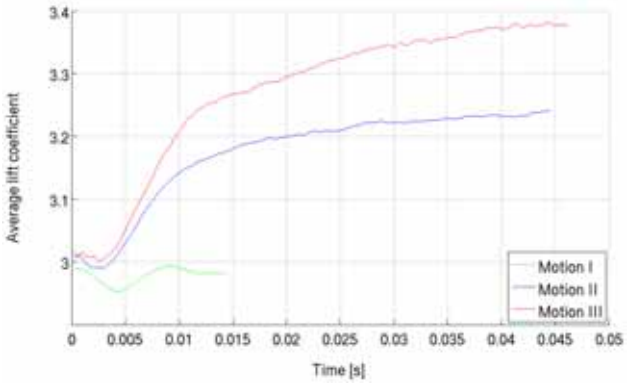

(a) Development of the lift coefficient in time.

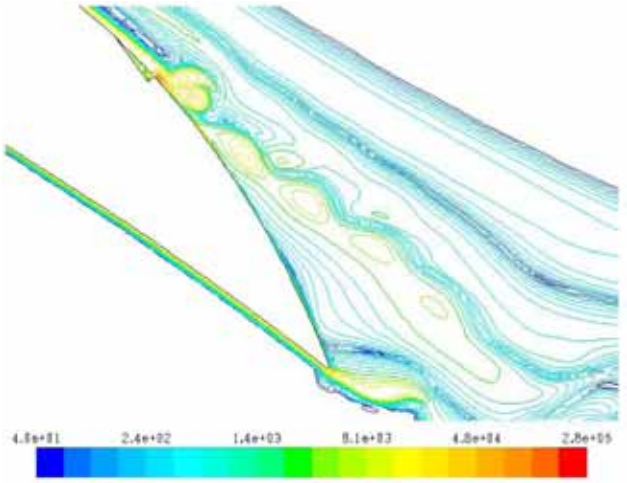

(b) Motion I

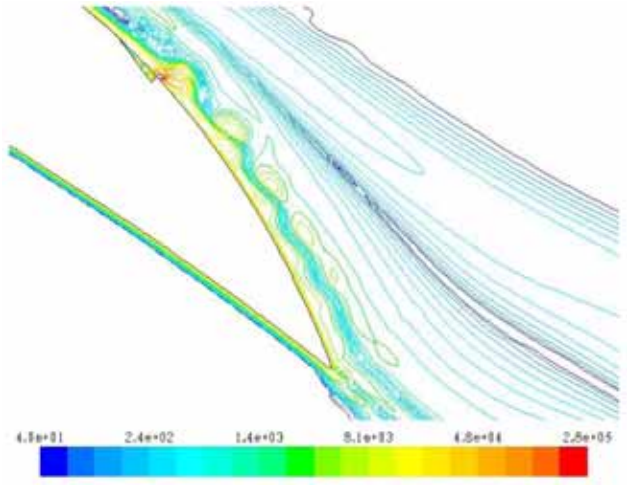

(c) Motion III

Fig. 20 Time history of the lift coefficient (a) and vorticity field over the flap (b,c) produced by the sharp cavity type fliperon (b,c). The contours indicate the vorticity magnitude in s^{-1}.

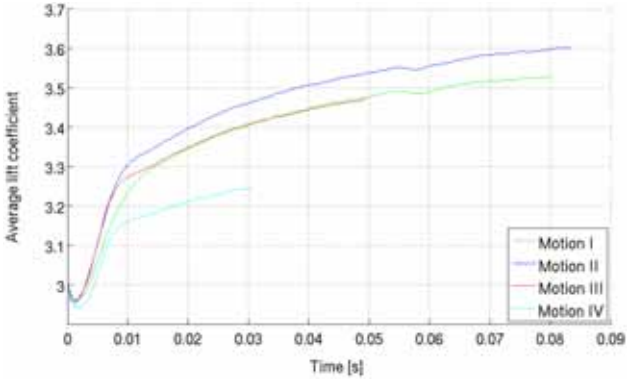

(a) Development of the lift coefficient in time.

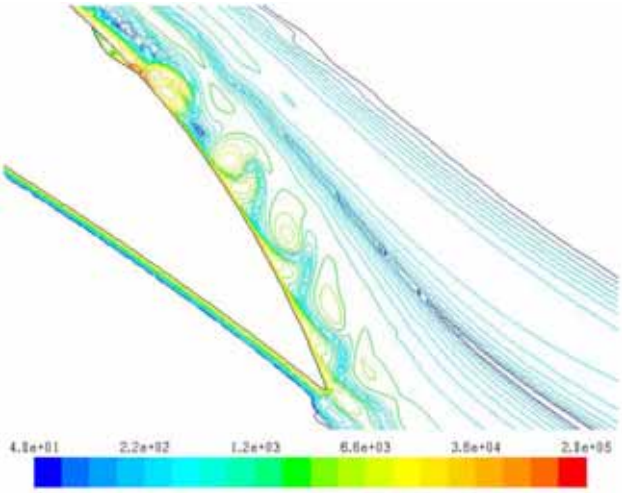

(b) Motion II

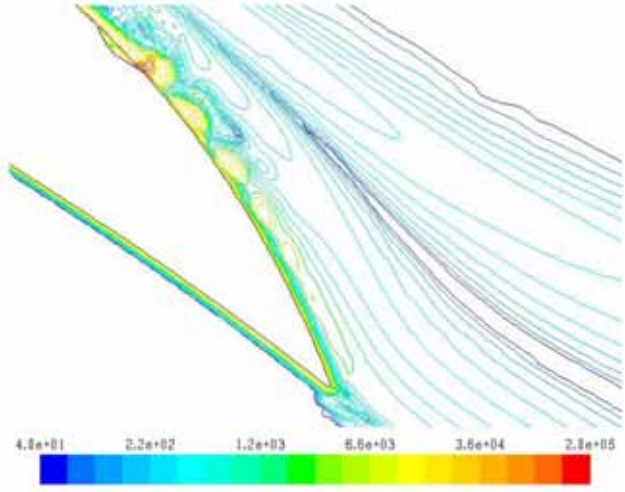

(c) Motion IV

Fig. 21 Time history of the lift coefficient (a) and vorticity field over the flap (b,c) produced by the smooth cavity type fliperon (b,c). The contours indicate the vorticity magnitude in s^{-1}.

Table 4 Overview of the resulting lift coecient increases from different fliperon geometries.

Motion #	Actuator type	c_μ	$\Delta C_L(\%)$
I ($F^+ = 4.0$)	Springboard	0.1171	8.0
	Sharp cavity	0.0198	0.0
	Smooth cavity	0.0872	18.8
II ($F^+ = 6.0$)	Springboard	0.2700	18.0
	Sharp cavity	0.0834	9.1
	Smooth cavity	0.1443	21.2
III ($F^+ = 8.0$)	Springboard	0.1065	13.7
	Sharp cavity	0.1497	16.8
	Smooth cavity		

electrical) drivers makes the system fragile

- they produce noise

In this respect the current development of (non-moving) plasma actuators for separation control may prove a much better approach.

5 Conclusion

Experiments and numerical analysis on surface excitation actuorors that were compared with vortex generators have been performed succesfully. It was shown that periodic surface excitation could eliminate separation completely in a typical setup of the flow over a ramp. Optimized conventional vortex generators with a height equal to the boundary layer thickness showed a smaller separation postponement effect. However it was noted that Micro-VG's (VG's with a height of $\frac{\delta}{2}$) were quite as effective as the actuator in their optimal configuration.

PIV measurements showed that periodic surface excitation eliminates flow separation by generation of a discrete vortex during upward motion. This vortex is composed of smaller scale structures with a high vorticity. When the actuator moves down, the vortex is stretched and convected with the flow.

From the numerical analysis of the flow over a two-dimensional wing flap model it was found that flow separation over the flap could be controlled by a surface mounted actuator (fliperon)

positioned ahead of the separation point. The perfomance of the actuator is strongly dependent on the applied actuator frequency and presence of a cavity below the fliperon. Although the separation control capabilities of the surface excitation actuator have been proven their application in practise may be impractible due to maintainabily, reliability and noise issues.

References

[1] Artois, K., "Active Separation Control by Periodic Excitation in an Adverse Pressure Gradient, Application of a Mechanical Actuator", Master's Thesis, University of Delft, May 2005.

[2] Greenblatt, D. and I. J. Wygnanski, I.J., "The control of ow separation by periodic excitation", Progress in Aerospace Sciences, 36:487-545, 2000.

[3] Seifert, A., "Separation Control at Flight Reynols Numbers: Lessons Learned and Future Directions", AIAA 2000-2542, Fluids 2000, 19-22 June 2000, Denver, CO

[4] Nishri, B. and Wygnanski, I., " Effects of periodic excitation on turbulent flow separation on a flap. AIAA Journal, 36(4):547-556, April 1998

[5] Seifert, A., Eliahu, S. and Greenblatt, D., "Use of piezoelectric actuators for airfoil separation control", AIAA Journal, 36(8):1535-1537, August 1998

[6] Veldhuis, L.L.M. and Artois, K., "Active Separation Control by Periodic Excitation in an Adverse Pressure Gradient", AIAA-2007-3917 25th AIAA Applied Aerodynamics Conference, Miami, FL, June 25-28, 2007

[7] Baragona, M. Unsteady Characteristics of Laminar Separation Bubbles, PHD thesis Delft Univerity of Technology, 2004.

[8] van Hest, B. F. A. Laminar-turbulent transition in boundary layers with adverse pressure gradient, PHD thesis Delft Univerity of Technology, 1996

[9] Schubauer, G. B., Spangenberg W. G. Mixing in boundary layers, J. of Aircraft Vol. 8:10-31,1960

[10] Taylor, H. D. Summary report on Vortex Generators, R-052809, United Aircraft Corporation, Research Department, March 1950

[11] Lin, J. C. & Robinson, S. K. & McGhee, R. J. & Valarezo, W. O. Separation Control on High-Lift Airfoils via Micro-Vortex Generators, J. of Aircraft Vol. 31, No.6, November-December 1994, p.1317-1323

[12] Seifert, A. Eliahu, S. Greenblatt, D. Wygnanski, I. Use of Piezoelectric Actuators for Airfoil Separation Control, AIAA Journal, Vol. 36, No. 8, August 1998.

[13] Osborn, R. F., Kota, S., Hetrick, J. A., Active ow controlusing using high frequency compliant structures, J. of Aircraft Vol. 41-3, may-june 2004.

[14] AGARD, A selection of experimental test cases for the validation of CFD codes. Advisory Report 303, 1, August 1994

[15] Dolle, T., Flap Performance Improvement by Surface Excitation - A numerical research into active flow control, MSc Thesis, Delft University of Technology, Faculty of Aerospace Engineering, 2009

Copyright Statement